

Hydrogen Bonding of 7,8-Dihydro-8-oxodeoxyguanosine with a Charged Residue in the Little Finger Domain Determines Miscoding Events in *Sulfolobus solfataricus* DNA Polymerase Dpo4^{*,§}

Received for publication, March 16, 2007, and in revised form, April 12, 2007. Published, JBC Papers in Press, April 27, 2007, DOI 10.1074/jbc.M702290200

Robert L. Eoff¹, Adriana Irimia¹, Karen C. Angel, Martin Egli, and F. Peter Guengerich²

From the Department of Biochemistry and Center in Molecular Toxicology, Vanderbilt University School of Medicine, Nashville, Tennessee 37232-0146

Sulfolobus solfataricus P2 DNA polymerase IV (Dpo4) has been shown to catalyze bypass of 7,8-dihydro-8-oxodeoxyguanosine (8-oxoG) in a highly efficient and relatively accurate manner. Crystal structures have revealed a potential role for Arg³³² in stabilizing the *anti* conformation of the 8-oxoG template base by means of a hydrogen bond or ion-dipole pair, which results in an increased enzymatic efficiency for dCTP insertion and makes formation of a Hoogsteen pair between 8-oxoG and dATP less favorable. Site-directed mutagenesis was used to replace Arg³³² with Ala, Glu, Leu, or His in order to probe the importance of Arg³³² in accurate and efficient bypass of 8-oxoG. The double mutant Ala³³¹Ala³³² was also prepared to address the contribution of Arg³³¹. Transient-state kinetic results suggest that Glu³³² retains fidelity against bypass of 8-oxoG that is similar to wild type Dpo4, a result that was confirmed by tandem mass spectrometric analysis of full-length extension products. A crystal structure of the Dpo4 Glu³³² mutant and 8-oxoG:C pair revealed water-mediated hydrogen bonds between Glu³³² and the O-8 atom of 8-oxoG. The space normally occupied by Arg³³² side chain is empty in the crystal structures of the Ala³³² mutant. Two other crystal structures show that a Hoogsteen base pair is formed between 8-oxoG and A in the active site of both Glu³³² and Ala³³² mutants. These results support the view that a bond between Arg³³² and 8-oxoG plays a role in determining the fidelity and efficiency of Dpo4-catalyzed bypass of the lesion.

Enzyme-catalyzed reactions are fundamental in biology (1–3). Certain elements of an enzymatic mechanism may be obvious once elucidated (*i.e.* required catalytic residues, prosthetic groups, the presence or absence of cofactors), and the relevance for function is readily discerned. In other instances, features of interest may be difficult to identify in the multitude of non-essential elements that often comprise enzyme-substrate interactions (4, 5). For example, nucleotide selection and subsequent incorporation by DNA polymerases have been described in great detail (6, 7), and the chemical components necessary for phosphoryl transfer are conserved across all domains of life and across all polymerase subfamilies. Yet, in the course of analyzing different polymerases it has become apparent that not all of these enzymes use the same mechanism(s) to define substrate specificity, a vital aspect of polymerase function (8).

The Y-family DNA polymerases appear to present a case of relaxed substrate selection, but the less accurate mode of copying template DNA is supplanted by the greater propensity of Y-family polymerases to effectively utilize damaged DNA as a substrate (9–12). Indeed, the ubiquitous nature of DNA damage, both endogenous and exogenous in origin, makes it necessary for the replisome to have some means of bypassing covalently modified DNA (13). Some general features unique to Y-family polymerases that are relevant to translesion DNA synthesis include an active site that leaves the newly formed base pair relatively unconstrained by protein-DNA interactions and employment of an additional domain termed the “little finger” or palm-associated domain (PAD), which has important contacts with the template DNA near the active site (14, 15). Other mechanistic features of the Y-family that likely contribute to effective partitioning between low and high-fidelity polymerases include low processivity, relatively slow forward rates of polymerization (k_{pol}), and the requirement for high dNTP concentrations to achieve maximum catalytic rates (*i.e.* “high” K_D , dNTP) (16–19). Previous work from our group has shown that a model Y-family polymerase, Dpo4 from *Sulfolobus solfataricus* P2, is able to bypass 8-oxoG,³ a major lesion arising from

* This work was supported by National Institutes of Health Grants R01 ES010375 (to F. P. G.), F32 CA119776 (to R. L. E.), P30 ES000267 (to F. P. G. and M. E.), and P01 ES05355 (to M. E.). The costs of publication of this article were defrayed in part by the payment of page charges. This article must therefore be hereby marked “advertisement” in accordance with 18 U.S.C. Section 1734 solely to indicate this fact.

§ This article was selected as a Paper of the Week.

§ The on-line version of this article (available at <http://www.jbc.org>) contains supplemental Figs. S1–S31 and Tables S1–S6 detailing a large portion of the LC-MS/MS results used to analyze the full-length extension by WT Dpo4 and the mutant enzymes, steady-state parameters for the Ala³³¹Ala³³² mutant, and x-ray density.

The atomic coordinates and structure factors (codes 2uvw, 2uvw, 2uvu, 2uvr) have been deposited in the Protein Data Bank, Research Collaboratory for Structural Bioinformatics, Rutgers University, New Brunswick, NJ (<http://www.rcsb.org/>).

¹ These authors contributed equally to this work.

² To whom correspondence should be addressed: Dept. of Biochemistry and Center in Molecular Toxicology, Vanderbilt University School of Medicine, 638 Robinson Research Bldg., 23rd and Pierce Ave., Nashville, TN 37232-0146. Tel.: 615-322-2261; Fax: 615-322-3141; E-mail: f.guengerich@vanderbilt.edu.

³ The abbreviations used are: 8-oxoG, 7,8-dihydro-8-oxodeoxyguanosine; Dpo4, DNA polymerase IV; CID, collision-induced dissociation; DTT, dithiothreitol; ESI, electrospray ionization; LC, liquid chromatography; MS, mass spectrometry; MS/MS, tandem mass spectrometry; pol, (DNA) polymerase; pol T7⁻, bacteriophage pol T7 (exonuclease-deficient); WT, wild type.

Role of Arg³³² in Dpo4 Bypass of 8-OxoG

oxidative stress, in a highly accurate and efficient manner (20). The kinetic parameters and LC-MS analysis of extension products indicated that Dpo4 was ~20-fold more efficient at insertion of dCTP opposite 8-oxoG relative to dATP insertion. X-ray crystal structures revealed that the 8-oxoG:A pair was in the *syn:anti* configuration, which allows A to form a Hoogsteen pair with 8-oxoG. Conversely, the 8-oxoG:C pair was in the Watson-Crick geometry and such a configuration appeared to be stabilized by either a hydrogen bond or an ion-dipole pair between the O-8 atom and the side chain of Arg³³². The importance of such an interaction was further confirmed by separate studies that observed a water-mediated hydrogen bond between Arg³³² and 8-oxoG (21).

Thermodynamically and geometrically the 8-oxoG:A pair is similar to a T:A pair. In isolated oligonucleotides the 8-oxoG:A pair decreases the T_m by 5.5 °C relative to T:A, and the T_m for the corresponding 8-oxoG:C pair is 16.9 °C lower than a G:C pair (22). The question then arises as to why Dpo4 retains high efficiency and fidelity during bypass of 8-oxoG. The role of Arg³³² in nucleotide selection during Dpo4-catalyzed bypass of 8-oxoG was investigated using a series of mutant enzymes. In an effort to determine what factors contribute to the stabilization of the 8-oxoG:C pair, site-directed mutagenesis was used to alter different chemical aspects of the Arg³³² side chain, including steric occupancy and hydrogen bonding potential. Transient-state kinetic and LC-MS/MS analyses were then combined with x-ray crystallographic studies to compare mutant-catalyzed bypass of 8-oxoG with wild type Dpo4.

EXPERIMENTAL PROCEDURES

Materials—Site-directed mutagenesis was performed using synthetic oligonucleotide primers and a QuikChange mutagenesis kit (Stratagene, La Jolla, CA). Wild type Dpo4 and all of the mutant enzymes were expressed in *Escherichia coli* and purified to electrophoretic homogeneity as described previously (23). All unlabeled dNTPs were obtained from Amersham Biosciences, and [γ -³²P]ATP was purchased from PerkinElmer Life Sciences. All oligonucleotides used in this work were synthesized by Midland Certified Reagent Co. (Midland, TX) and purified using high performance liquid chromatography by the manufacturer, with analysis by matrix-assisted laser desorption time-of-flight MS. The 13-base primer sequence used in the kinetic and mass spectral analyses was 5'-GGGGGAAGGATTC-3'. The 14-base primer sequences used in the indicated kinetic assays and the crystal structures were 5'-GGGGGAAGGATTC-3' for the 8-oxoG:C structure and 5'-GGGGGAAGGATTC-3' for the 8-oxoG:A structure. The template DNA sequence used in the kinetic and mass spectral assays and in the 8-oxoG:C and 8-oxoG:A structures was 5'-TCACXGAATCCTTCCCC-3', where X = G or 8-oxoG, as indicated. The DNA control template sequence used in the full-length extension assay (Fig. 1B) was 5'-TCATGGAATCCTTCCCC-3'.

Full-length Extension Assay—A ³²P-labeled primer was annealed to either an unmodified or adducted template oligonucleotide. Each reaction was initiated by adding dNTP·Mg²⁺ (each dNTP at 250 μ M and 5 mM MgCl₂) solution to a preincubated Dpo4-DNA complex (100 nM Dpo4 and 200 nM DNA).

The reaction was carried out at 37 °C in 50 mM Tris-HCl (pH 7.4) buffer containing 50 mM NaCl, 5 mM DTT, 100 μ g μ l⁻¹ bovine serum albumin, and 5% (v/v) glycerol. At the indicated time, 5- μ l aliquots were quenched with 50 μ l of 500 mM EDTA (pH 9.0). The samples were then mixed with 100 μ l of a 95% formamide/20 mM EDTA solution and separated on a 20% polyacrylamide (w/v)/7 M urea gel. Products were visualized and quantified using a phosphorimaging screen and Quantity OneTM software, respectively (Bio-Rad). Formation of an 18-base extension product from a 13-base primer was quantified by fitting the data to Equation 1,

$$f_{18mer}(t) = A \left(1 - \sum_{r=1}^n \frac{((k_{obs}t)^{r-1})}{(r-1)!} e^{-(k_{obs}t)} \right) \quad (\text{Eq. 1})$$

where A = amount of product formed during the first binding event between Dpo4 and DNA, k_{obs} = an observed rate constant defining nucleotide incorporation, n = number of incorporation events required to observe product formation, and t = time. All statistical values given indicate S.E.

Transient-state Kinetics—All pre-steady-state experiments were performed using a KinTek RQF-3 model chemical quench-flow apparatus (KinTek Corp., Austin, TX) with 50 mM Tris-HCl (pH 7.4) buffer in the drive syringes. All RQF experiments were carried out at 37 °C in a buffer containing 50 mM Tris-HCl (pH 7.4) buffer containing 50 mM NaCl, 5 mM DTT, 100 μ g μ l⁻¹ bovine serum albumin, and 5% (v/v) glycerol. Polymerase catalysis was stopped by the addition of 500 mM EDTA (pH 9.0). Substrate and product DNA was separated by electrophoresis on a 20% polyacrylamide (w/v)/7 M urea gel. The products were then visualized using a phosphorimaging device and quantitated using Quantity OneTM software. Results obtained under single-turnover conditions were fit to Equation 2,

$$y = A(1 - e^{-k_{obs}t}) \quad (\text{Eq. 2})$$

where A = product formed in first binding event, k_{obs} = rate constant defining polymerization under the conditions used for the experiment being analyzed, and t = time. Results obtained under conditions that allowed a second round of Dpo4-DNA binding and polymerase action were fit to Equation 3,

$$y = A(1 - e^{-k_{obs}t}) + k_{ss}t \quad (\text{Eq. 3})$$

where k_{ss} represents a steady-state velocity of nucleotide incorporation. To obtain an estimate of the nucleotide binding affinity for each mutant, the concentration of dNTP in the reaction mixture was varied, and pre-steady-state experiments were performed under excess enzyme conditions. The resulting rate constants, k_{obs} , were then plotted as a function of dNTP concentration, and the data were fit to the hyperbolic expression $k_{obs} = (k_{pol} \cdot [dNTP]) / ([dNTP] + K_{D,dNTP})$ using GraphPad Prism.

LC-MS/MS Analysis of Oligonucleotide Products from Dpo4 Reactions—Dpo4 (5 μ M) was preincubated with primer-template DNA (10 μ M), and the reaction was initiated by the addition of dNTP (1 mM each) and MgCl₂ (5 mM) in a final volume of 100 μ l. Dpo4 catalysis was allowed to proceed at 37 °C for 4 h in

50 mM Tris-HCl (pH 7.8 at 25 °C) buffer containing 50 mM NaCl, 1 mM DTT, 50 $\mu\text{g } \mu\text{l}^{-1}$ bovine serum albumin, and 5% glycerol (v/v). The reaction was terminated by extraction of the remaining dNTPs using a size-exclusion chromatography column (Bio-Spin 6 chromatography column, Bio-Rad). Concentrated stocks of Tris-HCl, DTT, and EDTA were added to restore the concentrations to 50, 5, and 1 mM, respectively. Next, *E. coli* uracil-DNA glycosylase (20 units, Sigma-Aldrich) was added, and the solution was incubated at 37 °C for 6 h to hydrolyze the uracil residue on the extended primer. The reaction mixture was then heated at 95 °C for 1 h in the presence of 0.25 M piperidine followed by removal of the solvent by centrifugation under vacuum. The dried sample was resuspended in 100 μl of H₂O for MS analysis.

LC-MS/MS analysis (23, 24) was performed on a Waters Aquity ultraperformance liquid chromatography system (UPLC; Waters, Milford, MA) connected to a Finnigan LTQ mass spectrometer (Thermo Fisher Scientific, Waltham, MA) operating in the ESI negative ion mode. An Aquity UPLC BEH octadecylsilane (C₁₈) column (1.7 μm , 1.0 \times 100 mm) was used with the following LC conditions: buffer A contained 10 mM NH₄CH₃CO₂ plus 2% CH₃CN (v/v), and buffer B contained 10 mM NH₄CH₃CO₂ plus 95% CH₃CN (v/v). The following gradient program was used with a flow rate of 150 $\mu\text{l min}^{-1}$: 0–3 min, linear gradient from 100% A to 97%A, 3% B (v/v); 3–4.5 min, linear gradient to 80% A, 20% B (v/v); 4–5.5 min, linear gradient to 100% B; 5–5.5 min, hold at 100% B; 5.5–6.5 min, linear gradient to 100% A; 6.5–9.5 min, hold at 100% A. The temperature of the column was maintained at 50 °C. Samples were injected with an autosampler system. ESI conditions were as follow: source voltage 4 kV, source current 100 μA , auxiliary gas flow rate setting 20, sweep gas flow rate setting 5, sheath gas flow setting 34, capillary voltage –49 V, capillary temperature 350 °C, tube lens voltage –90 V. MS/MS conditions were as follows: normalized collision energy 35%, activation Q 0.250, activation time 30 ms. The doubly (negatively) charged species were generally used for CID analysis. The calculations of the CID fragmentations of oligonucleotide sequences were done using a program linked to the Mass Spectrometry Group of Medicinal Chemistry at the University of Utah (www.medlib.med.utah.edu/massspec). The nomenclature used in supplemental Tables S1–S5 has been described previously (25).

Crystallization of Dpo4·DNA Complexes—R332A and R332E mutant crystallizations were performed in complex with DNA (18-mer template/14-mer primer duplex) and dGTP. The 18-mer template strand was 5'-TCAC(8-oxoG)GAATCCT-TCCCCC-3', and the 14-mer primer strand was 5'-GGGG-GAAGGATTCX-3' with the 3'-terminal nucleotide X being either A or C. The R332E(8-oxoG:C) structure was crystallized by the hanging drop vapor diffusion technique, using a mixture of 14% polyethylene glycol 4000 (w/v), 0.1 M calcium acetate, and 20 mM HEPES (pH 7.3) as reservoir. The three other mutant complexes were crystallized as described earlier (23). Only CaCl₂ was added to the protein-DNA-dGTP incubation mixture, and all buffers were Mg²⁺-free.

X-ray Diffraction Data Collection and Processing—The x-ray diffraction data sets for the four mutant·DNA·dGTP complexes

were collected on insertion device beamlines (5-ID, DND-CAT, and 17-ID, IMCA-CAT) at the Advanced Photon Source, Argonne, IL, at a temperature of 110 K, using a synchrotron radiation wavelength of 1.0 Å. Indexing and scaling were performed using X-GEN (26) (R332E(8-oxoG:A)), XDS (27) (R332E(8-oxoG:C), and R332A(8-oxoG:A)) or HKL2000 (28) (R332A(8-oxoG:C)). All four structures belong to the space group P2₁2₁2. The resulting data sets for the R332E(8-oxoG:A) and R332E(8-oxoG:C) complexes were of excellent quality, with values for R_{merge} of 4.7 and 5.3%, respectively. Data sets of slightly lower quality were obtained for the R332A(8-oxoG:A) and R332A(8-oxoG:C) complexes (R_{merge} values of 8.8 and 13.7%, respectively). CCP4 package programs including TRUNCATE (29) were used for further processing of the data.

Structure Determination and Refinement—The refined wild type Dpo4·dG complex (Protein Data Bank accession code 2c22 (20)) minus solvent molecules and dGTP was used as the starting model for R332A(8-oxoG:C). The initial position of the model was optimized by several rounds of rigid body refinement while gradually increasing the resolution of the diffraction data. The refined structure of the R332A(8-oxoG:C) complex served as the starting model for the other three crystals, and the locations of the individual models were optimized by rigid body refinement as described above.

Manual model rebuilding was done with the program TURBO-FRODO.⁴ The maps were computed using the σ_A -modified coefficients (30). Clear positive density for the Ca²⁺ ions and the dGTP was observed in the initial difference Fourier electron density maps of all four complexes. Also, unambiguous negative or positive density (regarding the initial model selected; see above) appeared for the mutated residues, which were then replaced with the correct residue type. The CNS package (crystallography NMR software) (31) was used for the refinement of the models by performing simulated annealing, gradient minimization, and refinement of individual isotropic temperature factors. The statistics of the refined models for all structures are summarized in Table 5, and representative electron density maps for the final models are depicted in the supplemental data section. The crystallographic figures were prepared using PyMOL.⁵

RESULTS

Primer Extension Past G and 8-OxoG Using All Four dNTPs—As a general measure of how Dpo4 catalysis opposite 8-oxoG is affected by mutating the Arg³³² residue, a time course was performed for each mutant in the presence of all four dNTPs (Fig. 1). An observed rate constant defining five incorporation events can be measured by following the appearance of the fully extended 18-mer primer and fitting the data to Equation 1, where $n = 5$ (Table 1). The Ala³³² and Glu³³² mutants were each ~2-fold faster at full-length extension opposite unmodified DNA than WT Dpo4 or the other mutants. However, WT Dpo4 was ~2–6-fold faster than any of the mutants at full-length extension opposite 8-oxoG. To address the potential

⁴ C. Cambillau and A. Roussel (1997) *Turbo Frodo*, Version OpenGL.1, Université Aix-Marseille II, Marseille, France.

⁵ W. L. DeLano (2002) *The PyMOL Molecular Graphics System*, www.pymol.org.

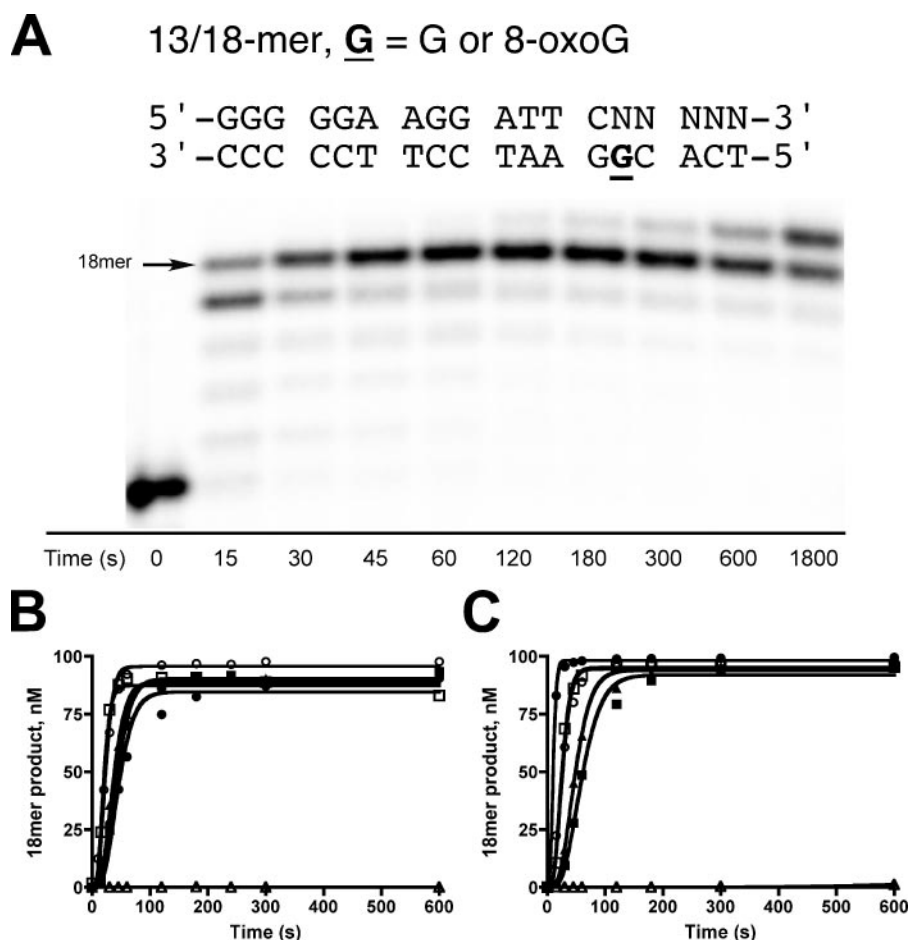


FIGURE 1. Comparison of full-length extension as catalyzed by wtDpo4 and Arg³³² mutants. A, the sequence of primer-template DNA and a representative gel of full-length extension experiments. WT Dpo4 (100 nM) catalysis opposite 8-oxoG-modified DNA (100 nM) in the presence of a 1 mM mixture of all four dNTPs is shown. All experiments were performed in the presence of 1 μ M unlabeled DNA (protein trap) to create true single-turnover conditions. B, formation of fully extended 18-mer product opposite unmodified DNA was quantified and plotted as a function of time for WT Dpo4 and the mutants (●), Ala³³² (○), Leu³³² (■), Glu³³² (□), His³³² (▲), and Ala³³¹Ala³³² (△). C, formation of fully extended 18-mer product opposite 8-oxoG-modified DNA was quantified and plotted as a function of time for WT Dpo4 (●) and the mutants Ala³³² (○), Leu³³² (■), Glu³³² (□), His³³² (▲), and Ala³³¹Ala³³² (△). The results were fit to Equation 1 (Table 1).

TABLE 1
Transient-state kinetic parameters describing full-length extension of 13/18-mer primer-template DNA

The experimental conditions were: [Dpo4] = 100 nM, [DNA] = 100 nM, [dNTP mix] = 1 mM, [13/18-mer trap] = 1 mM. ND, not determined due to lack of sufficient product formation.

Enzyme	k_{obs}	Template base	Product amplitude
	s^{-1}	nM	
WT	-G-	85 ± 3	0.10 ± 0.007
WT	-8-oxoG-	98 ± 1	0.48 ± 0.010
Ala ³³²	-G-	96 ± 1	0.21 ± 0.007
Ala ³³²	-8-oxoG-	95 ± 2	0.18 ± 0.009
Leu ³³²	-G-	90 ± 1	0.11 ± 0.002
Leu ³³²	-8-oxoG-	92 ± 2	0.08 ± 0.003
Glu ³³²	-G-	87 ± 2	0.24 ± 0.015
Glu ³³²	-8-oxoG-	94 ± 1	0.19 ± 0.006
His ³³²	-G-	89 ± 1	0.13 ± 0.003
His ³³²	-8-oxoG-	94 ± 1	0.10 ± 0.003
Ala ³³¹ Ala ³³²	-G-	ND	ND
Ala ³³¹ Ala ³³²	-8-oxoG-	ND	ND

contribution of Arg³³¹ to bypass of 8-oxoG, a double alanine mutant (Ala³³¹Ala³³²) was prepared. The Ala³³¹Ala³³² double mutant failed to extend the primer during the first binding

event, but full-length extension by the double mutant did occur under conditions that allowed multiple binding events (supplemental Fig. S1). It is important to note that in the absence of any other evidence, the exact identity of the fully extended products is unknown.

Analysis of Primer Incorporation/Extension Products Using LC-MS/MS with Dpo4 Extension Products—To identify the sequence of the full-length extension products (Fig. 1), LC-MS/MS analysis of the oligonucleotide products was used, as described previously (Fig. 2) (23, 24). Control reactions with unmodified DNA were performed. Accurate copying of the unmodified DNA template was reflected in the only product observed for each of the mutants, indicating that fidelity is unperturbed (>99% C incorporation, data not shown). The reactions with 8-oxoG were performed in triplicate to obtain a statistical evaluation of the mutant insertion spectrum (Table 2, supplemental Tables S1–S5, and supplemental Figs. S2–S30). All of the mutants catalyzed incorporation of C and A opposite 8-oxoG (Table 2). Some of the products had an additional A or C added to the 3' terminus of the primer in what is assumed to be a template-independent manner (blunt-end addition). The range of misincorporation was small (11.1 ± 0.4% A incorporation for Ala³³¹Ala³³² and 16.0 ± 0.8% A incorporation for His³³²). The trend in fidelity of 8-oxoG bypass predicted from the LC-MS/MS results was: Ala³³¹Ala³³² ≈ WT Dpo4 ≈ Glu³³² (highest C incorporation) > Leu³³² > Ala³³² ≈ His³³² (lowest C incorporation).

Transient-state Kinetic Analysis of Dpo4 Mutants and dCTP Incorporation Opposite 8-OxoG—Single-turnover experiments were performed with the concentration of nucleotide varied in order to provide an estimate of k_{pol} and $K_{D,dNTP}$ for each mutant (Fig. 3 and Table 3). The estimates obtained in the kinetic approaches highlight the first insertion event opposite 8-oxoG, as opposed to LC-MS/MS analysis, which was conducted under conditions that allow multiple rounds of binding and dissociation.

Dpo4 Ala³³² displays several interesting characteristics. The maximum forward rate of polymerization for Ala³³² (k_{pol}) was 4.4- and 4.9-fold faster than observed previously with WT Dpo4 for unmodified G and 8-oxoG-modified substrates, respectively (20). The Ala³³² mutant also displayed a higher affinity (lower $K_{D,dCTP}$) for dCTP when bound to the unmodi-

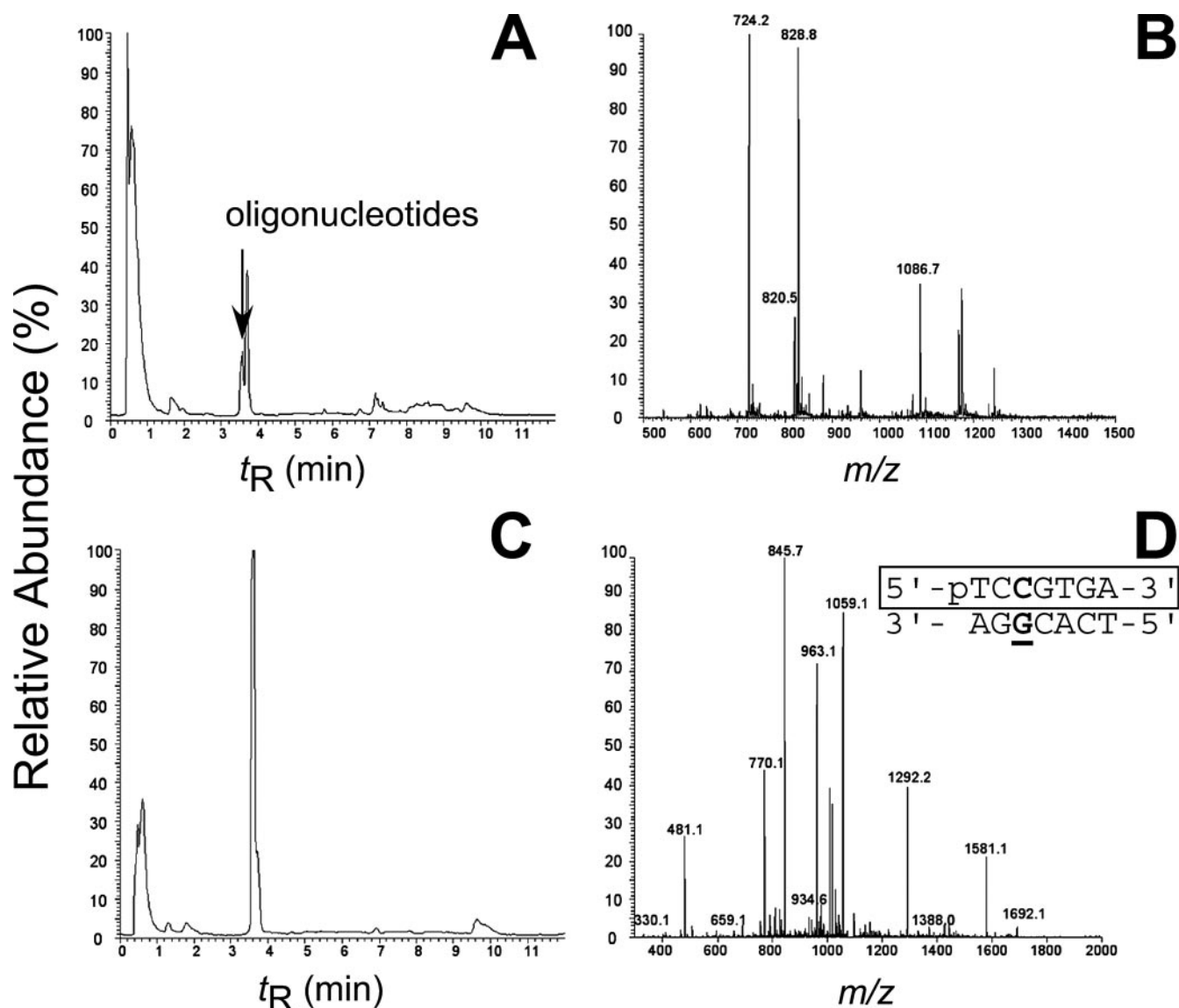


FIGURE 2. Identification of Dpo4 mutant-catalyzed full-length extension products by LC-MS/MS. *A*, total ion current trace of products derived from Ala³³²-catalyzed extension of 13/18-mer DNA containing 8-oxoG. *B*, ESI mass spectrum of the oligonucleotide peaks that elute at 3.4 min. *C*, total ion current trace of ion *m/z* 1087. *D*, CID mass spectrum of ion *m/z* 1087. "G" denotes 8-oxoG. This product contained C inserted opposite 8-oxoG and extended in an error-free manner.

TABLE 2

Summary of full-length extension products determined from LC-MS/MS analysis

Experiments were performed in triplicate ($n = 3 \pm \text{S.D.}$).

Product	% of total product					
	WT Dpo4	Ala ³³²	Glu ³³²	Leu ³³²	His ³³²	Ala ³³¹ Ala ³³²
5' - TCCGTGA - 3' 3' - AGGCACT - 5'	37.0 ± 3.0	30.8 ± 6.0	0.6 ± 0.5	21.6 ± 2.4	10.3 ± 0.5	61.7 ± 1.9
5' - TCCGTGAA - 3' 3' - AGGCACT - 5'	33.9 ± 1.8	44.1 ± 5.1	50.0 ± 0.1	56.3 ± 1.6	60.0 ± 0.7	6.5 ± 0.2
5' - TCCGTGAC - 3' 3' - AGGCACT - 5'	17.7 ± 1.0	9.5 ± 0.7	38.0 ± 0.9	7.8 ± 0.7	13.7 ± 0.1	23.9 ± 0.9
5' - TCAAGTGA - 3' 3' - AGGCACT - 5'	5.5 ± 0.7	7.2 ± 0.7	0.6 ± 0.1	3.2 ± 0.2	2.5 ± 0.2	4.6 ± 0.8
5' - TCAAGTGAA - 3' 3' - AGGCACT - 5'	5.9 ± 0.5	8.4 ± 1.4	10.9 ± 0.5	11.1 ± 1.2	13.5 ± 0.8	3.3 ± 0.2
Total C (%)	88.7 ± 0.4	84.3 ± 1.0	88.5 ± 0.5	85.7 ± 1.2	84.0 ± 0.8	88.9 ± 0.9
Total A (%)	11.3 ± 0.4	15.7 ± 1.0	11.5 ± 0.5	14.3 ± 1.2	16.0 ± 0.8	11.1 ± 0.9

fied DNA compared with the $K_{D,dCTP}$ measured for Ala³³²-catalyzed incorporation of dCTP opposite 8-oxoG. In the previous work with WT Dpo4, a greater affinity for dCTP was observed

for 8-oxoG-modified DNA ($K_{D,dCTP} = 27 \mu\text{M}$ for 8-oxoG; $K_{D,dCTP} = 420 \mu\text{M}$ for G). Comparison of WT Dpo4 and Ala³³² catalytic efficiency reveals that the mutant was 23-fold more

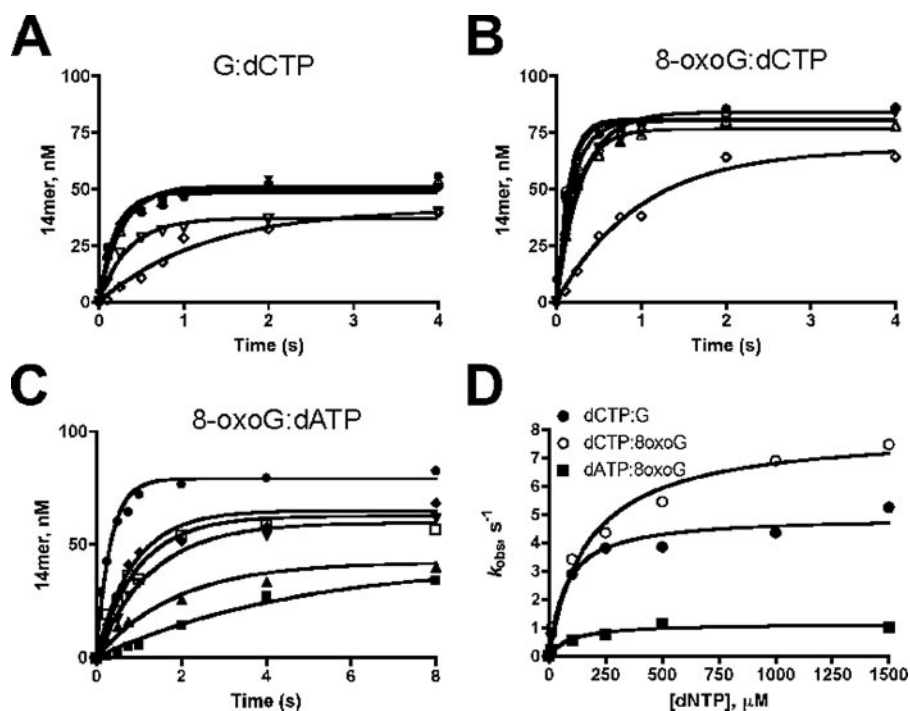


FIGURE 3. Determination of k_{pol} and $K_{D,\text{dNTP}}$ for Ala³³²-catalyzed incorporation opposite G and 8-oxoG. A, measurement of Ala³³²-catalyzed (200 nM) incorporation opposite G (100 nM) at varying concentrations of dCTP. B, measurement of Ala³³²-catalyzed (200 nM) incorporation opposite 8-oxoG (100 nM) at varying concentrations of dCTP. C, measurement of Ala³³²-catalyzed incorporation opposite 8-oxoG at varying concentrations of dATP. D, the observed rate of nucleotide incorporation was plotted as a function of dNTP concentration and fit to a quadratic equation to yield kinetic parameters (Table 3). Similar results were obtained for the other mutants.

TABLE 3
Transient-state kinetic parameters for dCTP and dATP incorporation opposite 8-oxoG

Enzyme	Primer/template	dNTP	k_{pol} s^{-1}	$K_{D,\text{dNTP}}$ mM
WT Dpo4	-G-	dCTP	1.1 ^a	420 ^a
	-8oxoG-	dCTP	1.6 ^a	27 ^a
Ala ³³²	-8oxoG-	dATP	1.5 ± 0.2	536 ± 152
	-G-	dCTP	4.9 ± 0.3	74 ± 23
Glu ³³²	-8oxoG-	dCTP	8.0 ± 0.5	171 ± 43
	-8oxoG-	dATP	1.2 ± 0.1	93 ± 43
Leu ³³²	-G-	dCTP	5.3 ± 0.8	742 ± 244
	-8oxoG-	dCTP	5.6 ± 0.3	165 ± 34
His ³³²	-8oxoG-	dATP	0.70 ± 0.1	349 ± 174
	-G-	dCTP	4.5 ± 0.6	520 ± 167
Ala ³³¹ Ala ³³²	-8oxoG-	dCTP	2.1 ± 0.3	110 ± 63
	-8oxoG-	dATP	0.48 ± 0.07	141 ± 89
Ala ³³¹ Ala ³³²	-G-	dCTP	4.0 ± 0.3	224 ± 68
	-8oxoG-	dCTP	7.3 ± 0.8	658 ± 170
Ala ³³¹ Ala ³³²	-8oxoG-	dATP	1.0 ± 0.2	293 ± 167
	-G-	dCTP	0.19 ± 0.01	15 ± 5
Ala ³³¹ Ala ³³²	-8oxoG-	dCTP	0.71 ± 0.04	30 ± 13
	-8oxoG-	dATP	ND ^b	ND ^b

^a Determined previously (20).

^b Not determined because of lack of sufficient product formation.

efficient at incorporation of C opposite G and 1.2-fold less efficient than WT Dpo4 in dCTP incorporation opposite 8-oxoG. In kinetic terms, the Ala³³² mutant was slightly more efficient at accurate bypass of G compared with 8-oxoG.

The Glu³³² mutant also exhibited slightly different kinetics from WT Dpo4. For instance, the k_{pol} value for dCTP incorporation opposite G was 4.8-fold faster than for WT Dpo4, similar to Ala³³². The k_{pol} value for dCTP incorporation opposite 8-oxoG was 3.5-fold faster than WT Dpo4 insertion of dCTP

opposite 8-oxoG. The lower $K_{D,\text{dCTP}}$ observed with WT Dpo4 for the 8-oxoG substrate relative to G was also apparent with the Glu³³² mutant, but the absolute affinity of the Glu³³² mutant for dCTP was diminished for both G and 8-oxoG. The catalytic efficiency of the Glu³³² mutant was 2.3-fold greater than WT Dpo4 for dCTP incorporation opposite G but 1.7-fold less efficient than WT Dpo4 for incorporation opposite 8-oxoG. Overall the Glu³³² mutant was ~5-fold more efficient at incorporating C opposite 8-oxoG compared with insertion opposite unmodified G.

The Leu³³² mutant can be hypothesized to serve as an intermediate between the Ala³³² and Glu³³² mutations in that the potential for hydrogen bonding between residue 332 and 8-oxoG is lost, but the steric occupancy of the Leu aliphatic side chain is retained, similar to the Glu³³² mutant. Pre-steady-state kinetic analysis revealed that the k_{pol} values for the Leu³³² mutant incorporation opposite G and

8-oxoG were 4.1- and 1.9-fold faster than those for WT Dpo4. The lower $K_{D,\text{dCTP}}$ when the Leu³³² mutant incorporates C opposite 8-oxoG (compared with $K_{D,\text{dCTP}}$ for insertion opposite G) was similar to both WT Dpo4 and the Glu³³² mutant, but the absolute value for Leu³³²-catalyzed bypass of 8-oxoG was increased relative to WT Dpo4. The Leu³³² mutant was still ~2-fold more efficient at incorporation of dCTP opposite 8-oxoG compared with G, but that difference was smaller than what is observed with WT Dpo4 and Glu³³².

The His³³² mutant exhibited faster forward rate constants relative to WT Dpo4. The k_{pol} values for the His³³² mutant incorporation opposite G and 8-oxoG were 3.6- and 4.6-fold faster than for WT Dpo4. The nucleotide binding affinity trend was opposite that of WT Dpo4, Glu³³², and Leu³³², with tighter dCTP binding during bypass of G. As in the case of Ala³³², the kinetic analysis indicated that His³³² inserted dCTP opposite G with slightly greater efficiency than opposite 8-oxoG.

The Ala³³¹Ala³³² double mutant had slower forward rate constants relative to WT Dpo4 for both G and 8-oxoG. The Ala³³¹Ala³³² double mutant-catalyzed insertion of dCTP opposite 8-oxoG was ~4-fold faster than dCTP insertion opposite G. The measured binding affinity of dCTP was tighter than that of WT Dpo4 for unmodified DNA, but the binding affinity of dCTP opposite 8-oxoG was similar to that observed for WT Dpo4. The catalytic efficiency for dCTP incorporation was increased ~4-fold for unmodified DNA and decreased ~2-fold for 8-oxoG-modified DNA.

Transient-state Kinetic Analysis of Dpo4 Mutants and dATP Incorporation Opposite 8-OxoG—Previous steady-state analysis indicated that Dpo4 is ~90-fold more efficient at dCTP

TABLE 4
Summary of catalytic efficiencies

Enzyme	$k_{\text{pol}}/K_{D,d\text{NTP}}$			
	G:C	8-oxoG:C	8-oxoG:A	8-oxoG:C/8-oxoG:A
WT Dpo4	0.003	0.059	0.003	20
Ala ³³²	0.066	0.047	0.013	4
Glu ³³²	0.007	0.034	0.002	17
Leu ³³²	0.009	0.020	0.003	7
His ³³²	0.018	0.011	0.003	4
Ala ³³¹ Ala ³³²	0.013	0.024	<0.00×	>20

incorporation opposite 8-oxoG compared with dATP incorporation opposite the lesion (20). Previous LC-MS/MS analysis of the full-length extension products was consistent with the steady-state results (~95% C and ~5% A incorporation). Pre-steady-state analysis of WT Dpo4 and mutant-catalyzed insertion of dATP opposite 8-oxoG was performed (Fig. 3 and Table 3). A useful comparison can be made by dividing the catalytic efficiency of dCTP incorporation by the efficiency of dATP incorporation ($[k_{\text{pol}}/K_{D,d\text{CTP}}]/[k_{\text{pol}}/K_{D,d\text{ATP}}]$). This ratio effectively measures the kinetic preference of dCTP over dATP in the concentration range of nucleotides used here (Table 4). The kinetic parameters indicate that WT Dpo4 was the most accurate enzyme tested, although Glu³³² also maintains a near wild type preference for dCTP (17-fold; Table 4). The remaining

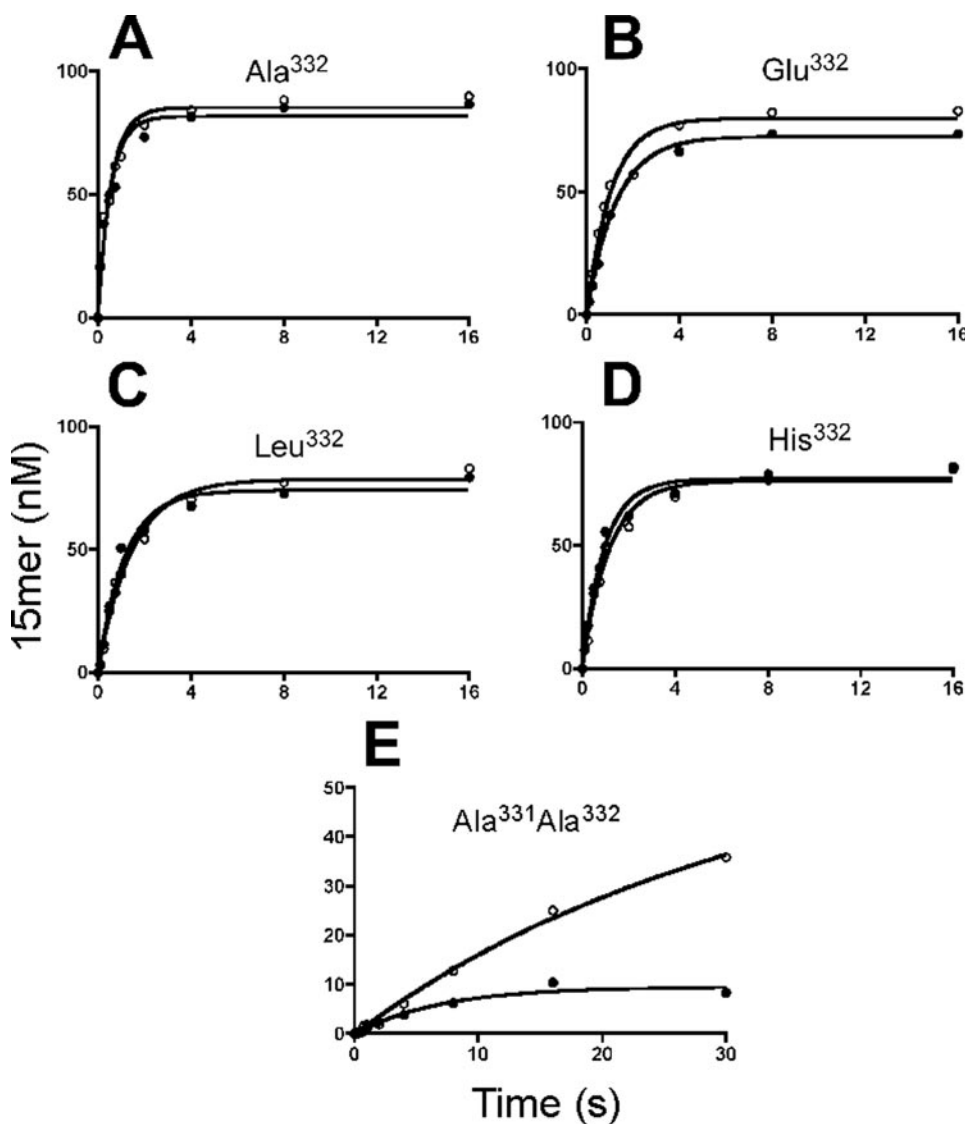


FIGURE 4. Next-base extension of 8-oxoG:C or 8-oxoG:A pair. Mutant Dpo4 (200 nM) was incubated with primer-template DNA (100 nM) containing 8-oxoG template annealed to a primer containing C (●) or A (○) paired opposite the lesion. The results for dGTP incorporation were then fit to Equation 3, and the following parameters were obtained. *Panel A*, Ala³³²: C (●) $A = 82 \pm 3$ nM, $k_{\text{obs}} = 1.8 \pm 0.3$ s⁻¹; A (○) $A = 85 \pm 3$ nM, $k_{\text{obs}} = 1.7 \pm 0.2$ s⁻¹. *Panel B*, Glu³³²: C (●) $A = 72 \pm 1$ nM, $k_{\text{obs}} = 0.8 \pm 0.05$ s⁻¹; A (○) $A = 80 \pm 3$ nM, $k_{\text{obs}} = 0.9 \pm 0.1$ s⁻¹. *Panel C*, Leu³³²: C (●) $A = 74 \pm 3$ nM, $k_{\text{obs}} = 0.8 \pm 0.1$ s⁻¹; A (○) $A = 79 \pm 2$ nM, $k_{\text{obs}} = 0.7 \pm 0.06$ s⁻¹. *Panel D*, His³³²: C (●) $A = 77 \pm 2$ nM, $k_{\text{obs}} = 1.0 \pm 0.1$ s⁻¹; A (○) $A = 76 \pm 3$ nM, $k_{\text{obs}} = 0.9 \pm 0.09$ s⁻¹. *Panel E*, Ala³³¹Ala³³²: C (●) $A = 9 \pm 1$ nM, $k_{\text{obs}} = 0.14 \pm 0.3$ s⁻¹; A (○) $A = 60 \pm 8$ nM, $k_{\text{obs}} = 0.031 \pm 0.006$ s⁻¹. The concentration of dGTP in all 10 experiments was 1 mM.

mutants all exhibited decreased substrate selectivity opposite 8-oxoG, indicating some disruption to the enzymatic properties that define high-fidelity bypass of 8-oxoG. Neither the Ala³³² nor the Leu³³² mutant is capable of forming a hydrogen bond with 8-oxoG. The His³³² residue is apparently ineffective at forming a hydrogen bond with 8-oxoG at pH 7.4 (the pK_a of the N-3 atom on the imidazole ring is presumably ~6.0), consistent with the view that hydrogen bonding between Arg³³² and the O-8 atom of 8-oxoG is important for accurate and efficient bypass of the lesion. The loss of fidelity observed with Ala³³² is driven by a much tighter binding of dATP relative to that observed with WT Dpo4 (Table 3), indicating that the Hoogsteen pair is better accommodated by the mutant. Likewise, the Leu³³² and His³³² mutants had lower $K_{D,d\text{ATP}}$ values than WT Dpo4 but not as low as Ala³³².

Of all of the enzymes tested, only the Ala³³¹Ala³³² double mutant failed to incorporate dATP opposite 8-oxoG in the pre-steady-state experiments. Steady-state experiments revealed that the Ala³³¹Ala³³² double mutant inserted dCTP opposite 8-oxoG with an ~200-fold greater efficiency than it did dATP (supplemental Table S6). The overall steady-state efficiency for dCTP insertion opposite 8-oxoG was decreased ~12-fold relative to WT Dpo4, and the steady-state efficiency of dATP incorporation was decreased ~27-fold relative to WT Dpo4.

TABLE 5
Crystal data and refinement parameters for the ternary (protein-DNA-dGTP) complexes of Dpo4 mutants

APS, Advanced Photon Source; DND-CAT, DuPont-Northwestern-Dow Collaborative Access Team; r.m.s.d., root mean square deviation; c-v, cross-validation.

Parameter	R332E(8-oxoG:A)	R332E(8-oxoG:C)	R332A(8-oxoG:A)	R332A(8-oxoG:C)
Crystal data				
X-ray source	APS (DND-CAT)	APS (DND-CAT)	APS (DND-CAT)	APS (IMCA-CAT)
Beamline	ID-5	ID-5	ID-5	ID-17
Detector	MARCCD	MARCCD	MARCCD	Quantum CCD
Wavelength (Å)	1.00	1.00	1.00	1.00
Temperature (K)	110	110	110	110
No. of crystals	1	1	1	1
Space group	P2 ₁ 2 ₁ 2			
Unit cell (<i>a</i> , <i>b</i> , <i>c</i> ; Å)	96.77,103.72,52.91	95.77,103.72,53.03	95.13,104.12,52.94	94.72,104.19,52.72
Resolution range (Å)	32.258–2.092	29.323–2.20	29.260–2.70	46.078–2.9
Highest resolution shell ^a	(2.17–2.09)	(2.28–2.2)	(2.8–2.70)	(3.0–2.9)
No. of measurements	105,683 (6,277)	175,452 (17,731)	75,984 (8,047)	50,447 (3,377)
No. of unique reflections	29,759 (2,221)	27,480 (2,697)	14,782 (1,532)	11,732 (965)
Redundancy	3.45 (2.8)	6.38 (6.57)	5.14 (5.25)	4.3 (3.5)
Completeness (%)	92.3 (70.2)	99.1 (98.6)	97.9 (98.9)	98.3 (89.0)
<i>R</i> _{merge} ^b	4.71 (43.66)	5.3 (43.8)	8.8 (55.9)	13.7 (60.7)
Signal to noise (<i>I</i> /σ ^c)	12.433 (1.5)	23.61 (4.41)	14.25 (2.71)	8.72 (1.80)
Solvent content (%)	54.7	55.3	54.2	55.5
Refinement				
Model composition (asymmetric unit)				
No. amino acid residues	341	342	342	341
No. water molecules	224	181	93	70
No. Ca ²⁺ ions	3	3	3	3
No. template nucleotides	17	15	17	17
No. primer nucleotides	14	14	14	14
No. dGTP	1	1	1	1
<i>R</i> _f ^c (%)	24.87	22.76	21.56	23.21
<i>R</i> _{free} ^d (%)	27.31	25.71	26.96	26.54
Estimated coordinate error (Å)				
Luzatti plot	0.33	0.30	0.37	0.43
Luzatti plot (c-v)	0.38	0.35	0.50	0.47
σA plot	0.44	0.27	0.52	0.54
σA plot (c-v)	0.47	0.24	0.62	0.57
Temperature factors				
Wilson plot (Å ²)	44.15	41.73	75.74	91.41
Mean isotropic (Å ²)	46.12	40.32	54.31	49.42
r.m.s.d. in temperature factors				
Bonded main chain atoms (Å ²)	1.38	1.37	1.37	1.21
Bonded side chain atoms (Å ²)	1.94	1.96	1.94	1.68
r.m.s.d. from ideal values				
Bond lengths (Å)	0.006	0.006	0.007	0.006
Bond angles (°)	1.28	1.30	1.31	1.10
Dihedral angles (°)	21.28	21.29	21.23	21.80
Improper angles (°)	1.48	1.48	1.50	1.48

^a Values in parentheses correspond to the highest resolution shells.

^b $R_{\text{merge}} = \frac{\sum_{hkl} \sum_j |I_{hkl} - \langle I_{hkl} \rangle|}{\sum_{hkl} \sum_j I_{hkl}}$ where the outer sum (*hkl*) is taken over the unique reflections.

^c $R_f = \frac{\sum_{hkl} |F_o(hkl) - k| |F_c(hkl)|}{\sum_{hkl} |F_o(hkl)|}$ where $|F_o(hkl)|$ and $|F_c(hkl)|$ are the observed and calculated structure factor amplitudes, respectively.

^d *R*_{free} is same as for *R*_f for the set of reflections (5% of the total) omitted from the refinement process.

Mutant Dpo4-catalyzed Extension beyond 8-OxoG Paired with C or A—The next-base extension of 8-oxoG:C and 8-oxoG:A pairs was measured by performing pre-steady-state experiments at a high concentration of the incoming dGTP (Fig. 4). All of the single mutants extended the 8-oxoG:C and 8-oxoG:A pairs in a similar manner, suggesting that next-base extension was relatively unaffected by the identity of the pair being extended. The rate of extension of the 8-oxoG:C pair was decreased for all four mutants relative to the *k*_{pol} value for dCTP incorporation opposite 8-oxoG (Fig. 4 compared with Table 3), indicating that some inhibition occurred when 8-oxoG:C entered the post-insertion site. Mutant-catalyzed extension of the 8-oxoG:A pair proceeded at rates similar to those measured for insertion of dATP opposite 8-oxoG (Fig. 4 compared with Table 3). The Ala³³¹Ala³³² double mutant extended the C:8-oxoG pair, but the rate and the amplitude of product formation were both decreased. The double mutant extended the A:8-oxoG pair, but the rate was very slow.

R332A Mutant-DNA Complex Structures—The structures of the Ala³³² mutant were determined in complex with a DNA

duplex (18-mer template and 14-mer primer) containing either an 8-oxoG:A or an 8-oxoG:C base pair and an incoming dGTP at the active site (termed R332A(8-oxoG:A) and R332A(8-oxoG:C), respectively; Table 5 and supplemental Fig. S31). Both the R332A(8-oxoG:A) and the R332A(8-oxoG:C) structure represent type I complexes (11). The template C located 5' to 8-oxoG is accommodated inside the active site of both the R332A(8-oxoG:A) and the R332A(8-oxoG:C) structures and pairs with dGTP at the replication site (Fig. 5, A and B). The 8-oxoG pairs with the 3'-terminal base of the primer at the post-insertion (−1) site. The short side chain of Ala³³² allows considerable space for accommodating 8-oxo-G:C or 8-oxoG:A pairs (Fig. 6, A and B). 8-oxoG is in a *syn* conformation in the R332A(8-oxoG:A) complex and forms a Hoogsteen pair with A. In this complex the O-8 atom forms a water-mediated hydrogen bond with Tyr¹² (Fig. 5A). The R332A(8-oxoG:C) complex shows the 8-oxoG residue in an *anti* conformation and forming a Watson-Crick paired with C. Lys⁷⁸ forms a water-mediated hydrogen bond to the N-2 of 8-oxoG (Fig. 5B). Such water-mediated hydrogen bonding interactions involving Tyr¹² or Lys⁷⁸ were

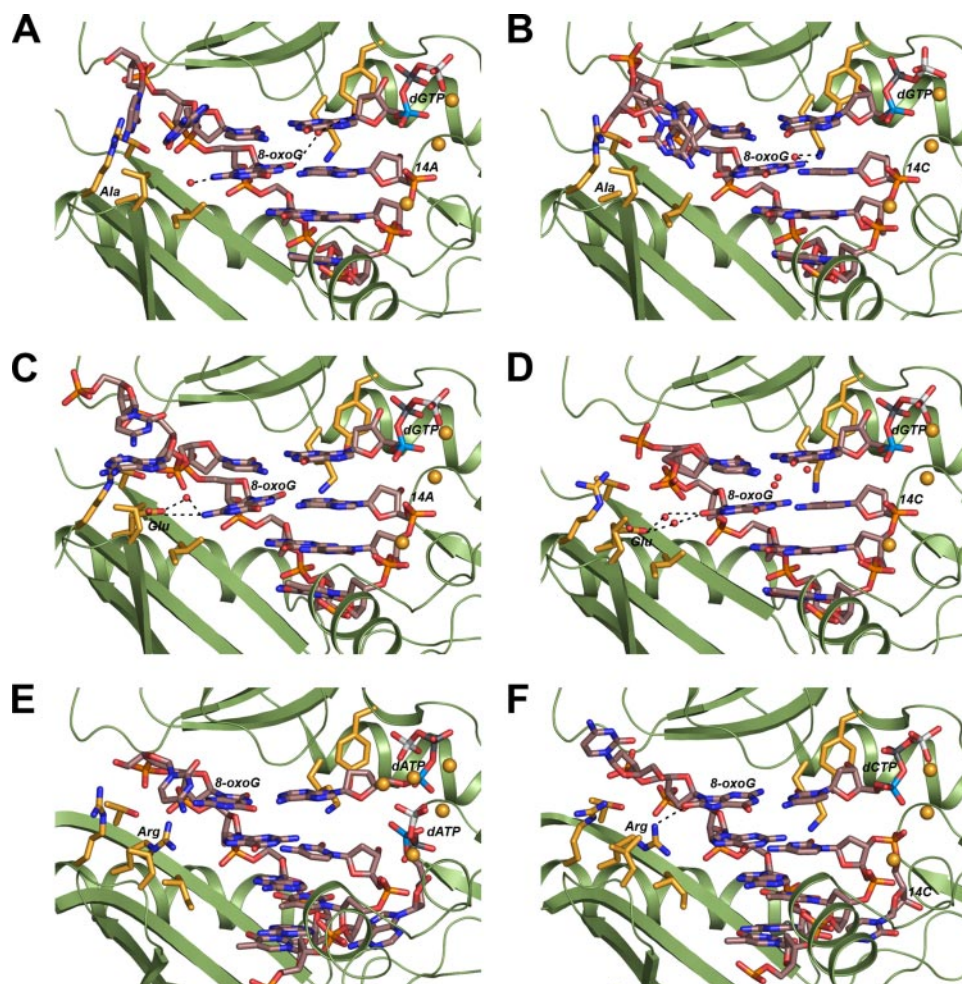


FIGURE 5. **Hydrogen bonding interactions between Dpo4 and the 8-oxoG lesion.** A, *R332A(8-oxoG:A)*; B, *R332A(8-oxoG:C)*; C, *R332E(8-oxoG:A)*; D, *R332E(8-oxoG:C)*; E, wild type 8-oxoG:dATP; F, wild type 8-oxoG:dCTP. The protein is shown with schematic α -helices and β -strands. The DNA duplex and selected Dpo4 residues are shown in stick mode. Ca^{2+} ions and water molecules are shown as yellow and red spheres, respectively, and hydrogen bonds as dashed lines.

not observed in the WT Dpo4 complexes (Fig. 5, E and F) (20). There, the 8-oxoG pairs with the dNTP at the replicative position. The Tyr¹² and Lys⁷⁸ side chains are directed toward the base pair in the -1 position both in the WT Dpo4 and mutant structures (Fig. 5). Therefore, the presence of the water-mediated hydrogen bonds observed in case of the R332A mutant structures suggests that these residues may play a role in translocation of the primer-template duplex and may not be critical with regard to the insertion event.

R332E Mutant-DNA Complex Structures—The Glu³³² mutant protein was complexed with an 18-mer template-14-mer primer DNA duplex containing either 8-oxoG:A or 8-oxoG:C pair at the active site and an incoming dGTP (termed *R332E(8-oxoG:A)* and *R332E(8-oxoG:C)*, respectively; supplemental Fig. S31). As with the complexes of Dpo4 alanine mutants above, the template C located 5' to 8-oxoG pairs with dGTP and 8-oxoG pairs with the 3'-terminal base of the primer at the -1 site. 8-oxoG pairs in the Hoogsteen mode with A in the *R332E(8-oxoG:A)* structure (Fig. 5C). Here, Glu³³² engages in a direct but relatively long hydrogen bond (3.46 Å) as well as a water-mediated interaction with the exocyclic amino group

N-2 of 8-oxoG. The *R332E(8-oxoG:C)* structure reveals a 8-oxoG:C pair in a Watson-Crick configuration with the O-8 oxygen linked to Glu³³² via two water molecules (Fig. 5D). The side chain of Glu³³² fills most of the space near the 8-oxoG base (Fig. 6, C and D). The available space is thus clearly reduced compared with the Ala³³² mutant structures but still is more open than in the WT Dpo4 structures. The presence of the long side chain of Arg³³² in WT Dpo4 (Fig. 6, E and F) may influence the choice of the inserted nucleotide. Steric hindrance and resulting repulsive interactions may take place in the case of the wild type 8-oxoG:dATP complex, leading to a destabilization of the Hoogsteen pair between 8-oxoG and dATP. Conversely, formation of a hydrogen bond between Arg³³² and O-8 can be expected to stabilize the Watson-Crick 8-oxoG:dCTP pair in the wild type 8-oxoG:dCTP complex (20), thus providing a rationalization of the preferred incorporation of C opposite 8-oxoG by Dpo4.

DISCUSSION

Mechanisms of cellular dysfunction, including carcinogenesis and aging, are caused, in part, by covalent modification of DNA (13, 32). 8-oxoG is an important lesion to

consider because it is widely prevalent and known to be mutagenic. Many of the DNA polymerases studied *in vitro* incorporate a large fraction of A opposite 8-oxoG relative to C (33–39). Some polymerases, such as yeast pol η (40, 41) and RB69 (42), preferentially insert dCTP opposite 8-oxoG, but the ability of Dpo4 to bypass 8-oxoG in a manner that is not only accurate but also more efficient than catalysis opposite unmodified DNA makes it unique among the DNA polymerases studied to date (20). Previous work suggested that a hydrogen bond between Arg³³² and the O-8 atom of 8-oxoG facilitates the increased efficiency of Dpo4 catalysis (20, 21). The role of Arg³³² in facilitating bypass efficiency was examined by studying the structure and mechanism of four mutant enzymes.

There are two major points to consider when discussing Dpo4-catalyzed bypass of 8-oxoG. First, the accuracy (or fidelity) of the reaction is high. The role of Arg³³² may be to help stabilize the *anti* conformation of the purine ring system of 8-oxoG, which would favor the 8-oxoG:C Watson-Crick-like pair over the 8-oxoG:A Hoogsteen pair. The second major point to consider is the matter of enzyme efficiency. Does Arg³³² play a predominant role in increasing the efficiency of

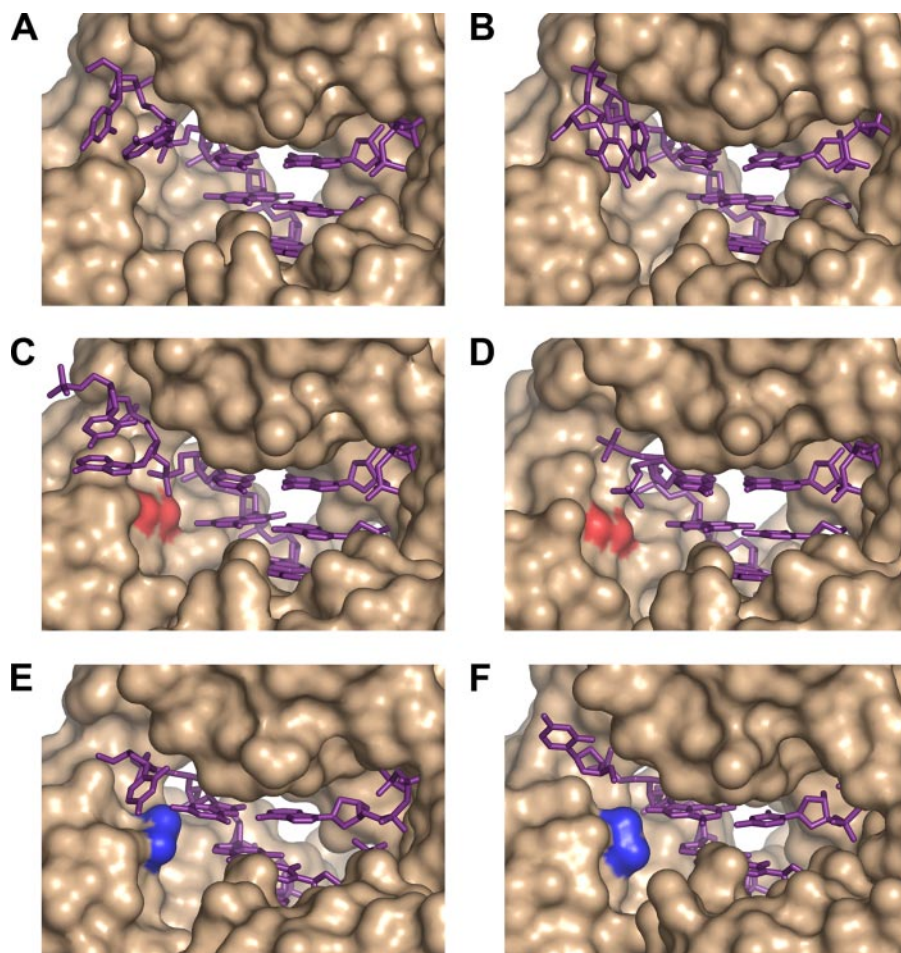


FIGURE 6. **Molecular surface representation of Dpo4 mutants illustrating the available space around the 8-oxoG lesion.** A, R332A(8-oxoG:A); B, R332A(8-oxoG:C); C, R332E(8-oxoG:A); D, R332E(8-oxoG:C); E, WT Dpo4 (8-oxoG:A); F, WT Dpo4 (8-oxoG:C). Dpo4 surfaces are colored in light brown, and DNA duplexes and dNTPs are shown in magenta. The red (panels C and D) and blue (panels E and F) patches on the protein surface indicate the positions of the Glu³³² and Arg³³² residues, respectively.

8-oxoG bypass, or is efficiency determined by several interactions between Dpo4 and the template DNA?

On the issue of fidelity, changing the identity of the Arg³³² residue does not result in obvious changes to Dpo4 catalysis opposite unmodified DNA (Fig. 1 and LC-MS data not shown). Relatively subtle changes in fidelity were observed in LC-MS/MS analysis of the full-length extension products for 8-oxoG-modified DNA (Table 2). The Glu³³² mutant exhibits fidelity that is very similar to WT Dpo4 (~11% A incorporation). With the exception of the Ala³³¹Ala³³² double mutant, the other mutants incorporated more A, indicating that some interaction was lost that moved the equilibrium between accurate and mutagenic bypass of 8-oxoG toward incorporation of A. The kinetic parameters are consistent with the LC-MS/MS results. The predicted trend in fidelity of 8-oxoG bypass is as follows: WT Dpo4 ≈ Ala³³¹Ala³³² (highest C incorporation) > Glu³³² > Leu³³² > Ala³³² ≈ His³³² (lowest C incorporation). One interesting comparison here is between the apparent preference, as determined by kinetic efficiency, and the products identified by LC-MS/MS. The kinetic parameters indicate that WT Dpo4 and the Glu³³² would insert ~5–6% A compared with ~15% A for Leu³³² and ~27% A for the Ala³³² and His³³²

mutants. Yet, the full-length extension products differ by only ~4%. When considered alone, the kinetic parameters suggest an important role for hydrogen bonding capability at position 332, but when considered in the context of both kinetics and the LC-MS/MS results, a less than definitive role for a hydrogen bond between residue 332 and the O-8 atom of 8-oxoG emerges in the determination of Dpo4 fidelity opposite the lesion. The differences highlighted by the kinetic results may be diminished in the LC-MS/MS results, because the full-length extension assays are performed under conditions that allow multiple catalytic turnovers, which may reflect events that are not measured during single nucleotide incorporation (*i.e.* product dissociation, translocation, and/or next-base extension).

Regarding the fidelity of 8-oxoG bypass, the Ala³³¹Ala³³² mutant presents some interesting features. Both kinetic and LC-MS/MS analyses indicate that the double mutant has even higher fidelity than WT Dpo4. However, it is also apparent that the processivity of the double mutant is severely impeded, most likely at the step following dNTP insertion opposite 8-oxoG. A crystal structure was solved of the

double mutant in complex with the C:8-oxoG pair, but the little finger domain is disordered, which makes it difficult to discern why the double mutant retains such high fidelity opposite 8-oxoG (data not shown). On the other hand, the full-length extension results with the Ala³³¹Ala³³² double mutant clearly show an effect upon Dpo4 processivity. Indeed, all of the enzymes tested here are slower at next-base extension of the 8-oxoG:C pair, indicating the importance of positively charged residues in the little finger domain during the Dpo4 translocation step. Such a view is consistent with previous structural work showing that Arg³³² maintained contact with 8-oxoG even when the template base is shifted into the post-insertion site of a type II structure (20).

The second major point to consider is the efficiency of Dpo4-catalyzed bypass of 8-oxoG. In this regard, the Glu³³² mutant is most similar to WT Dpo4. The Glu³³² mutant is 5-fold more efficient at inserting dCTP opposite 8-oxoG compared with G. The Leu³³² mutant is 2-fold more efficient inserting dCTP opposite 8-oxoG compared with G, but the Ala³³² and His³³² mutants are slightly more efficient at inserting dCTP opposite G. With the exception of Ala³³², which inserts dCTP opposite G with ~20-fold greater efficiency than WT Dpo4 (Table 4), the

gap between efficiency of G and 8-oxoG bypass is caused primarily by a decrease in bypass efficiency opposite 8-oxoG (Table 4). As with the issue of fidelity, the differences in efficiency are not large, but the Glu³³² mutant is the only one of these mutants capable of effectively forming a hydrogen bond with 8-oxoG, and it is the most similar to WT Dpo4 in kinetic terms.

The fact that the Glu³³² mutant is similar to WT Dpo4 contradicted our initial hypothesis that the negatively charged side chain of Glu³³² would move 8-oxoG into the Hoogsteen mode. The crystal structures reveal how the similarities between WT Dpo4 and Glu³³² are maintained. A water-mediated hydrogen bond is formed between the carboxylic acid moiety of Glu³³² and the O-8 atom of 8-oxoG (Fig. 5C). The Glu³³² mutant also forms a hydrogen bond with the N-2 exocyclic amino group of 8-oxoG when the 8-oxoG:A Hoogsteen pair is formed (Fig. 5D). No such interaction is observed in the structure of WT Dpo4 and the 8-oxoG:A Hoogsteen pair (20), but it is unclear what effect a hydrogen bond between Glu³³² and the N-2 amino group of 8-oxoG has upon dATP insertion, as the efficiency is not increased relative to WT Dpo4 (Table 4).

An interesting difference between WT Dpo4 and the Ala³³² mutant is the increased proclivity to insert dATP, which reduces the fidelity of the Ala³³² mutant. The Ala³³² mutant crystal structures (Fig. 6, A and B) reveal an empty space in the region normally occupied by Arg³³² in WT Dpo4. The Arg³³¹ residue maintains contact with the template DNA to the 5'-side of the 8-oxoG lesion and does not change conformation to replace Arg³³². The increased ability of the Ala³³² mutant to insert dATP opposite 8-oxoG may be related to the *syn/anti* equilibrium in the Dpo4 active site. A larger space could be more accommodating to the 8-oxoG:A Hoogsteen pair, as evidenced by the relatively low $K_{D,dATP}$ measured for Ala³³² insertion of dATP opposite 8-oxoG (Table 3).

In comparing the mechanism for Dpo4-catalyzed bypass of 8-oxoG with other DNA polymerases, an important similarity to bacteriophage pol T7⁻ is observed. The crystal structure of pol T7⁻ in ternary complex with a 8-oxoG:ddCTP pair revealed that Lys⁵³⁶ is in position to form a hydrogen bond with the O-8 atom of 8-oxoG (33). The side chain of Lys⁵³⁶ moves 3 Å relative to the position observed in a superimposed structure of pol T7⁻ bound to unmodified DNA. The stabilization of 8-oxoG by a hydrogen bond bears obvious resemblance to Dpo4, but it is estimated that pol T7 inserts A opposite 8-oxoG in ~30% of incorporation events, even when exonuclease activity is present (33). Insertion of dCTP opposite 8-oxoG by pol T7⁻ is inhibited ~180-fold relative to insertion of dCTP opposite G (comparing pre-steady-state data) (36). Both the level of dATP incorporation and the catalytic inhibition of pol T7⁻ is in direct contrast to what has been observed with Dpo4. The stabilization of 8-oxoG by Lys⁵³⁶ in the pol T7⁻ structure is apparently not substantial enough to overcome other factors, *i.e.* a geometrically intolerant active site and kinking of the template DNA backbone, to facilitate high efficiency and high fidelity during T7⁻-catalyzed bypass of 8-oxoG.

A sequence alignment of Dpo4 with *Saccharomyces cerevisiae* pol η based on secondary structure predicts that a histidine

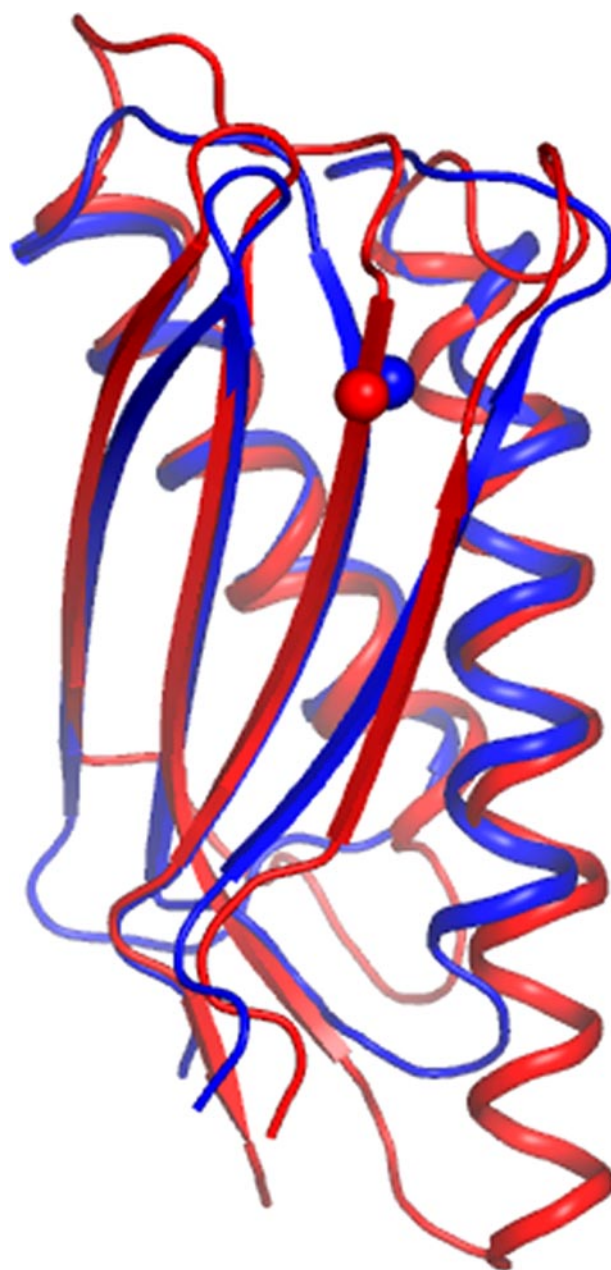


FIGURE 7. Superposition of the little finger domains of wild type Dpo4 and *S. cerevisiae* Pol η. Dpo4 and Pol η (Protein Data Bank accession code 1jih (44)) are represented schematically with secondary structure elements colored blue and red, respectively. The positions of the C α atoms of Arg³³² (Dpo4) and Lys⁴⁹⁸ (Pol η) are shown as spheres.

residue should be found in the region occupied by Arg³³² (11). However, a structure-based alignment of the little finger domain from the two proteins suggests that Arg³³² is replaced by a lysine (Lys⁴⁹⁸) in *S. cerevisiae* pol η (Fig. 7). The results presented here may be consistent with our structure-based alignment, because the His³³² mutant has the lowest fidelity of all of the mutants tested here, whereas yeast pol η is known to bypass 8-oxoG with relatively high fidelity (40). If our structure-based alignment is correct then the electrostatic interaction between the little finger domain and 8-oxoG may also be important for high-fidelity translesion synthesis opposite 8-oxoG by pol η.

Role of Arg³³² in Dpo4 Bypass of 8-OxoG

The hydrogen bond between Arg³³² and 8-oxoG is probably not the only factor affecting Dpo4 fidelity/efficiency during bypass of the lesion. There are, in fact, several other charged residues in the little finger that make important contacts with the phosphate backbone of DNA (including Arg²⁴², Arg²⁴⁷, Lys²⁷⁵, Arg²⁹⁸, Arg³³¹, and Arg³³⁶). The array of positively charged residues may help guide the *anti* conformation of 8-oxoG into and out of the active site of Dpo4, consistent with interactions predicted by computational studies (43). Changing the nature one of these residues does not appear to dramatically alter enzyme efficiency, even if it is the residue that contacts 8-oxoG during insertion opposite the lesion. Another possible reason for the small changes in fidelity and efficiency observed with the mutants emerges when one superimposes WT Dpo4 structure and either the Glu³³² or Ala³³² mutant structures. In the all of the structures, Ala⁴² engages in a C(H)₃ ··· π interaction with the templating base that helps to define the “roof” of the Dpo4 active site. When 8-oxoG is in the *anti* conformation, ready to pair with the incoming dCTP in a Watson-Crick mode, the “stacking” interaction with Ala⁴² is more favorable than when 8-oxoG assumes the *syn* conformation. In the *syn* orientation the six-member ring of 8-oxoG extends out into the major groove and does not interact with Ala⁴². Interestingly, the active site of T7⁻ has a glycine residue (Gly⁵²⁷; Protein Data Bank accession code 1TK0) in place of alanine. In pol T7⁻ the contact between Gly⁵²⁷ and the template base is less intimate, with only a single hydrogen atom directed toward the nucleobase. It is possible that the interaction with Ala⁴² in WT Dpo4 favors the *anti* conformation of 8-oxoG and in combination with the Arg³³² hydrogen bond in WT Dpo4 effectively seals the preference for incorporation of dCTP. In the case of the Ala³³² mutant, the hydrogen bond at position 332 is absent, but the stacking interaction between 8-oxoG and Ala⁴² may still promote a relatively high-fidelity mechanism of bypass. Of the mutants tested here, Glu³³² maintains catalytic properties during bypass of 8-oxoG that are most similar to WT Dpo4. A water-mediated hydrogen bond between Glu³³² and the O-8 atom of 8-oxoG provides further evidence that Dpo4 does use a hydrogen bond with the O-8 atom of 8-oxoG as an electrostatic “handle” that participates in increasing the fidelity of bypass and, to some extent, as a means of increasing catalytic efficiency.

Acknowledgments—We thank P. S. Pallan and Z. Wawrzak for assistance with x-ray data collection and K. Trisler for help in preparation of the manuscript. Use of the Advanced Photon Source was supported by the U. S. Department of Energy, Basic Energy Sciences, Office of Science, under Contract W-31-109-Eng-38. The DuPont-Northwestern-Dow Collaborative Access Team (DND-CAT) Synchrotron Research Center at the Advanced Photon Source (Sector 5) is supported by E. I. DuPont de Nemours & Co., the Dow Chemical Company, the National Science Foundation, and the State of Illinois. Use of the IMCA-CAT Beamline 17-ID at the Advanced Photon Source was supported by the companies of the Industrial Macromolecular Crystallography Association through a contract with the Center for Advanced Radiation Sources at the University of Chicago.

REFERENCES

1. Boyer, P. D. (1960) *Annu. Rev. Biochem.* **29**, 15–44
2. Gerlt, J. A., and Babbitt, P. C. (2001) *Annu. Rev. Biochem.* **70**, 209–246
3. Hammes-Schiffer, S., and Benkovic, S. J. (2006) *Annu. Rev. Biochem.* **75**, 519–541
4. DeLucia, A. M., Chaudhuri, S., Potapova, O., Grindley, N. D., and Joyce, C. M. (2006) *J. Biol. Chem.* **281**, 27286–27291
5. McElhinny, S. A., Stith, C. M., Burgers, P. M., and Kunkel, T. A. (2007) *J. Biol. Chem.* **282**, 2324–2332
6. Johnson, K. A. (1993) *Annu. Rev. Biochem.* **62**, 685–713
7. Kunkel, T. A. (2004) *J. Biol. Chem.* **279**, 16895–16898
8. Joyce, C. M., and Benkovic, S. J. (2004) *Biochemistry* **43**, 14317–14324
9. Choi, J.-Y., Stover, J. S., Angel, K. C., Chowdhury, G., Rizzo, C. J., and Guengerich, F. P. (2006) *J. Biol. Chem.* **281**, 25297–25306
10. Ling, H., Boudsocq, F., Plosky, B. S., Woodgate, R., and Yang, W. (2003) *Nature* **424**, 1083–1087
11. Ling, H., Boudsocq, F., Woodgate, R., and Yang, W. (2001) *Cell* **107**, 91–102
12. Ling, H., Sayer, J. M., Plosky, B. S., Yagi, H., Boudsocq, F., Woodgate, R., Jerina, D. M., and Yang, W. (2004) *Proc. Natl. Acad. Sci. U. S. A.* **101**, 2265–2269
13. Friedberg, E. C., Walker, G. C., Siede, W., Wood, R. D., Shultz, R. A., and Ellenberger, T. (2006) *DNA Repair and Mutagenesis*, 2nd Ed., ASM Press, Washington, D. C.
14. Prakash, S., Johnson, R. E., and Prakash, L. (2005) *Annu. Rev. Biochem.* **74**, 317–353
15. Yang, W. (2003) *Curr. Opin. Struct. Biol.* **13**, 23–30
16. Fiala, K. A., and Suo, Z. (2004) *Biochemistry* **43**, 2116–2125
17. Fiala, K. A., and Suo, Z. (2004) *Biochemistry* **43**, 2106–2115
18. Washington, M. T., Johnson, R. E., Prakash, S., and Prakash, L. (1999) *J. Biol. Chem.* **274**, 36835–36838
19. Washington, M. T., Prakash, L., and Prakash, S. (2001) *Cell* **107**, 917–927
20. Zang, H., Irimia, A., Choi, J.-Y., Angel, K. C., Loukachevitch, L. V., Egli, M., and Guengerich, F. P. (2006) *J. Biol. Chem.* **281**, 2358–2372
21. Rechkoblit, O., Malinina, L., Cheng, Y., Kuryavyi, V., Broyde, S., Geacintov, N. E., and Patel, D. J. (2006) *PLoS Biol.* **4**, e11
22. McAuley-Hecht, K. E., Leonard, G. A., Gibson, N. J., Thomson, J. B., Watson, W. P., Hunter, W. N., and Brown, T. (1994) *Biochemistry* **33**, 10266–10270
23. Zang, H., Goodenough, A. K., Choi, J.-Y., Irimia, A., Loukachevitch, L. V., Kozekov, I. D., Angel, K. C., Rizzo, C. J., Egli, M., and Guengerich, F. P. (2005) *J. Biol. Chem.* **280**, 29750–29764
24. Eoff, R. L., Irimia, A., Egli, M., and Guengerich, F. P. (2007) *J. Biol. Chem.* **282**, 1456–1467
25. Christian, N. P., Reilly, J. P., Mokler, V. R., Wincott, F. E., and Ellington, A. D. (2001) *J. Am. Soc. Mass Spectrom.* **12**, 744–753
26. Howard, A. J. (2000) *Crystallographic Computing 7: Proceedings from the Macromolecular Crystallographic Computing School*, Oxford University Press, Oxford, UK
27. Kabsch, W. (1988) *J. Appl. Crystallogr.* **21**, 916–924
28. Otwinowski, Z., and Minor, W. (1997) *Methods Enzymol.* **276**, 307–326
29. French, G. S., Wilson, K. S. (1978) *Acta Crystallogr. Sect. A* **34**, 517–525
30. Vellieux, F. M., and Dijkstra, B. W. (1997) *J. Appl. Crystallogr.* **30**, 396–399
31. Brunger, A. T., Adams, P. D., Clore, G. M., DeLano, W. L., Gros, P., Grosse-Kunstleve, R. W., Jiang, J. S., Kuszewski, J., Nilges, M., Pannu, N. S., Read, R. J., Rice, L. M., Simonson, T., and Warren, G. L. (1998) *Acta Crystallogr. Sect. D Biol. Crystallogr.* **54**, 905–921
32. Ames, B. N. (1979) *Science* **204**, 587–593
33. Brieba, L. G., Eichman, B. F., Kokoska, R. J., Double, S., Kunkel, T. A., and Ellenberger, T. (2004) *EMBO J.* **23**, 3452–3461
34. Einolf, H. J., and Guengerich, F. P. (2001) *J. Biol. Chem.* **276**, 3764–3771
35. Einolf, H. J., Schnetz-Boutaud, N., and Guengerich, F. P. (1998) *Biochemistry* **37**, 13300–13312
36. Furge, L. L., and Guengerich, F. P. (1997) *Biochemistry* **36**, 6475–6487
37. Hsu, G. W., Ober, M., Carell, T., and Beese, L. S. (2004) *Nature* **431**, 217–221

38. Lowe, L. G., and Guengerich, F. P. (1996) *Biochemistry* **35**, 9840–9849
39. Shibutani, S., Takeshita, M., and Grollman, A. P. (1991) *Nature* **349**, 431–434
40. Carlson, K. D., and Washington, M. T. (2005) *Mol. Cell. Biol.* **25**, 2169–2176
41. Haracska, L., Yu, S. L., Johnson, R. E., Prakash, L., and Prakash, S. (2000) *Nat. Genet.* **25**, 458–461
42. Freisinger, E., Grollman, A. P., Miller, H., and Kisker, C. (2004) *EMBO J.* **23**, 1494–1505
43. Wang, Y., Arora, K., and Schlick, T. (2006) *Protein Sci.* **15**, 135–151
44. Trincao, J., Johnson, R. E., Escalante, C. R., Prakash, S., Prakash, L., and Aggarwal, A. K. (2001) *Mol. Cell* **8**, 417–426